

See discussions, stats, and author profiles for this publication at: <https://www.researchgate.net/publication/14025459>

Refined structure of villin 14T and a detailed comparison with other actin-severing domains

ARTICLE *in* PROTEIN SCIENCE · JUNE 1997

Impact Factor: 2.85 · DOI: 10.1002/pro.5560060608 · Source: PubMed

CITATIONS

31

READS

12

3 AUTHORS, INCLUDING:



Michelle A Markus
Harvard Medical School
26 PUBLICATIONS 424 CITATIONS

[SEE PROFILE](#)



Gerhard Wagner
Harvard Medical School
523 PUBLICATIONS 35,366 CITATIONS

[SEE PROFILE](#)

Refined structure of villin 14T and a detailed comparison with other actin-severing domains

MICHELLE A. MARKUS,^{1,3} PAUL MATSUDAIRA,² AND GERHARD WAGNER¹

¹Committee on Higher Degrees in Biophysics, Harvard University, and the Department of Biological Chemistry and Molecular Pharmacology, Harvard Medical School, 240 Longwood Avenue, Boston, Massachusetts 02115

²Whitehead Institute for Biomedical Research, Nine Cambridge Center, and the Department of Biology, Massachusetts Institute of Technology, Cambridge, Massachusetts 02142

(RECEIVED January 27, 1997; ACCEPTED March 11, 1997)

Abstract

Villin 14T is the amino terminal actin monomer binding domain from the actin-severing and bundling protein villin. Its structure has been determined in solution using heteronuclear multidimensional nuclear magnetic resonance (NMR) spectroscopy (Markus MA, Nakayama T, Matsudaira P, Wagner G. 1994. Solution structure of villin 14T, a domain conserved among actin-severing proteins. *Protein Science* 3:70–81). An additional nuclear Overhauser effect (NOE) spectroscopy data set, acquired using improved gradient techniques, and further detailed analysis of existing data sets, produced an additional 601 NOE restraints for structure calculations. The overall fold does not change significantly with the additional NOE restraints but the definition of the structure is improved, as judged by smaller deviations among an ensemble of calculated structures that adequately satisfy the NMR restraints. Some of the side chains, especially those in the hydrophobic core of the domain, are much more defined. This improvement in the detail of the solution structure of villin 14T makes it interesting to compare the structure with the crystal structure of gelsolin segment 1, which shares 58% sequence identity with villin 14T, in an effort to gain insight into villin 14T's weaker affinity for actin monomers. Villin 14T has smaller side chains at several positions that make hydrophobic contacts with actin in the context of gelsolin segment 1. The structure is also compared with the structure of the related actin-severing domain, severin domain 2.

Keywords: actin-binding proteins; gelsolin segment 1; modular proteins; nuclear magnetic resonance spectroscopy; severin domain 2; solution structure

Villin is a member of a family of actin-severing and capping proteins, built from three or six repeats of a conserved domain (Matsudaira & Janmey, 1988). These proteins not only sever and cap actin filaments in the presence of calcium, they also bind to actin monomers and nucleate filament growth. Actin filaments are uncapped by the addition of polyphosphoinositides, providing a

mechanism for the regulation of the severing proteins' activities. Villin is unique among the actin-severing proteins in that it contains a seventh domain, referred to as the headpiece, required for bundling actin filaments to form the scaffolding for microvilli on the surface of absorptive cells (Arpin et al., 1988; Bazari et al., 1988). Compared to gelsolin, another member of the actin-severing protein family, villin requires higher calcium concentrations for severing activity (Janmey & Matsudaira, 1988), and measurements of calcium binding by the first domain of villin (villin 14T) put the dissociation constant for the intramolecular site in the millimolar range (Markus et al., 1994a). Furthermore, the first domain of villin (villin 14T) binds to actin monomers somewhat more weakly than the first domain of gelsolin (gelsolin segment 1). (Compare Kwiatkowski et al., 1985, and Janmey & Matsudaira, 1988.) These observations bring into question whether villin actually displays its severing activity *in vivo*, as a mechanism for regulating actin under extreme circumstances, or whether the actin filament binding component of the severing activity has been combined with the actin filament binding activity of the seventh domain to create primarily an actin-bundling protein (Finidori et al., 1992).

Reprint requests to: Gerhard Wagner, Department of Biological Chemistry and Molecular Pharmacology, Harvard Medical School, 240 Longwood Avenue, Boston, Massachusetts 02115; e-mail: wagner@heindall.med.harvard.edu.

³Present address: Molecular Structural Biology Unit, National Institute of Dental Research, 30 Convent Drive, Room 132, Bethesda, Maryland 20892-4320.

Abbreviations: 2D, two-dimensional; COSY, correlation spectroscopy; HMQC, heteronuclear multiple quantum coherence; HSQC, heteronuclear single quantum coherence; NMR, nuclear magnetic resonance; NOE, nuclear Overhauser effect; NOESY, nuclear Overhauser effect spectroscopy; RMSD, root-mean-square deviation; $\langle \text{RMSD} \rangle$, average root-mean-square deviation; TOCSY, total correlation spectroscopy; villin 14T, the amino-terminal 126 amino acid residues from the chicken epithelial sequence for the protein villin.

Although the conserved domain is repeated to build actin-severing proteins of six domains, including villin and gelsolin, or three domains, such as severin, the domain apparently functions differently in different contexts. Thus, isolated domains 1 and 4 are observed to bind to actin monomers (Bryan, 1988; Pope et al., 1995) whereas linked domains 2 and 3 bind to actin filaments (Yin et al., 1988). The minimum fragment of gelsolin that displays severing activity includes domains 1 and 2 (Kwiatkowski et al., 1989).

Detailed structural information is becoming available for these proteins. The three-dimensional structure of gelsolin segment 1 in a complex with actin has been solved by X-ray crystallography (McLaughlin et al., 1993). The structure of the first domain of villin has been solved in solution by NMR (Markus et al., 1994a), as has the structured core of the seventh domain (C. J. McKnight, pers. comm.). The structure of severin domain 2 in solution is also available (Schnuchel et al., 1995). These studies have revealed that the conserved repeated domain has a unique fold, comprised of both β -sheet and α -helix, observed so far only in the actin-severing proteins and the single-domain actin regulating protein destrin (Hatanaka et al., 1996). Many of the residues within the most strongly conserved region contribute to the hydrophobic core of the molecule and to the turns between elements of secondary structure and thus are conserved for structural rather than functional reasons. Calcium is bound in two places in the gelsolin segment 1-actin co-crystal, an intramolecular site, with ligands from side chains from the second helix and a loop between two β -strands as well as from two backbone carbonyls, and an intermolecular site, with some ligands from the actin monomer (McLaughlin et al., 1993). Chemical shift evidence suggests similar binding sites in villin 14T (Markus et al., 1994a) and severin domain 1 (Schnuchel et al., 1995).

We have improved our original solution structure for villin 14T by adding over 600 additional NOE restraints and by subjecting the final distance geometry-derived structures to minimization using a potential energy function supplemented with terms to enforce experimental restraints. At this level of refinement, we compare the structures of villin 14T, gelsolin segment 1, and severin domain 2 in detail to look for clues to explain differences in their function. Specifically, we have looked for residues that can explain severin domain 2's inability to bind actin monomers and villin 14T's weaker binding compared to gelsolin segment 1. Differences in the hydrophobic patch that contacts actin seem to be the key, as described below.

Results

Extent of NOE assignments

Of the 1398 NOE crosspeaks that have been assigned, about 38% were assigned in either or both the ^{15}N NOESY HMQC and ^{15}N NOESY HSQC, 21% from the ^{13}C NOESY HMQC, and 41% from the 2D data sets. Virtually all of the peaks in the ^{15}N NOESY HMQC and the ^{15}N NOESY HSQC have been assigned. Efforts have been made to assign all the peaks in the 2D NOESY in D_2O , which has better resolution and sensitivity than the original 2D NOESY in H_2O . However, a few peaks remain unassigned due to redundancies in the proton chemical shifts and overlap of NOE crosspeaks.

Structure calculations and residual violations of restraints

The NMR data that provide restraints for structure calculations are summarized in Table 1. The methods used to obtain these data are

Table 1. Summary of data used in structure calculations

Restraint type	Number of restraints
Assigned NOE crosspeaks	1,398
NOE distance restraints (total)	1,321
Interproton distances	
Intraresidue	73
Inter-residue sequential ($ i - j = 1$)	422
Inter-residue medium range ($2 \leq i - j \leq 4$)	200
Inter-residue long range ($ i - j > 4$)	626
Hydrogen bond distances	86
Dihedral angles	
ϕ ($C_{(i-1)}-\text{N}_i-\text{C}_{\alpha i}-\text{C}_i'$)	67
χ_1 ($\text{N}_i-\text{C}_{\alpha i}-\text{C}_{\beta i}-\text{C}_{\gamma i}$)	53
Stereospecific assignments	
β methylene	42
γ terminal methyl groups for valine	8 of 9
δ terminal methyl groups for leucine	5 of 7

summarized in Materials and methods. A complete list of the restraints is available from the Protein Data Bank, ID code R2VIKMR. Based on these restraints, structures were calculated with the distance geometry program DG-II (Havel, 1991) and subjected to restrained minimization in X-PLOR (Brünger, 1992). Backbone atom representations of eleven refined distance geometry structures are superimposed in Figure 1A.

The overall fold of villin 14T, shown in Figure 1B, consists of a central β -sheet decorated with helices and a short parallel sheet, as previously reported. In the central five-stranded β -sheet, the first four strands ($\beta 2$, $\beta 1$, $\beta 4$, and $\beta 5$) are antiparallel and strand $\beta 6$ is parallel to $\beta 5$. When determined by the Kabsch and Sander criteria (Kabsch & Sander, 1983), the endpoints for the strands vary slightly in each of the calculated structures; the maximum ranges are 17–23 for $\beta 1$, 29–31 for $\beta 2$, 44–52 for $\beta 4$, 57–65 for $\beta 5$, and 94–98 for $\beta 6$. At the end of strand $\beta 6$, there is a tight β -turn, but the extended strand turns toward helix $\alpha 3$ instead of forming an additional hydrogen-bonded strand in the central β sheet. On one side of the sheet, helix $\alpha 1$ runs roughly antiparallel to helix $\alpha 2$ (71–88). Helix $\alpha 1$ is not well defined, but residues 3–6 and 8–10 are helical by the Kabsch and Sander criteria in several structures and the $^3J_{\text{HNH}\alpha}$ constants are small for residues 3–6, suggestive of helix. On the other side of the sheet, helix $\alpha 3$ (residues 103–109) cuts across the central β -sheet and a short two-stranded parallel β -sheet packs alongside it. The parallel β -sheet only meets the strict geometric criteria for a sheet in one structure; nevertheless, it can be recognized through the pattern of slowly exchanging amide protons, the large $^3J_{\text{HNH}\alpha}$ coupling constants, interstrand NOE crosspeaks, and the low RMSD among the calculated structures in this region, with strand $\beta 3$ (residues 38–40) and strand $\beta 7$ (115–117). Between strand $\beta 2$ in the central sheet and strand $\beta 3$ in the parallel β -sheet, residues 33–36 resemble one turn of helix, with small values of $^3J_{\text{HNH}\alpha}$ for 33–34 and 36 and somewhat reduced amide exchange rates at 33 and 35–36.

Statistics reflecting the quality of the structures are summarized in Table 2. For the 11 best structures from a calculation of 20, residual NOE restraint violations were small, with no violations above 0.5 Å in any structure. The number of violations above 0.3 Å, per structure on average, is less than one, and the number

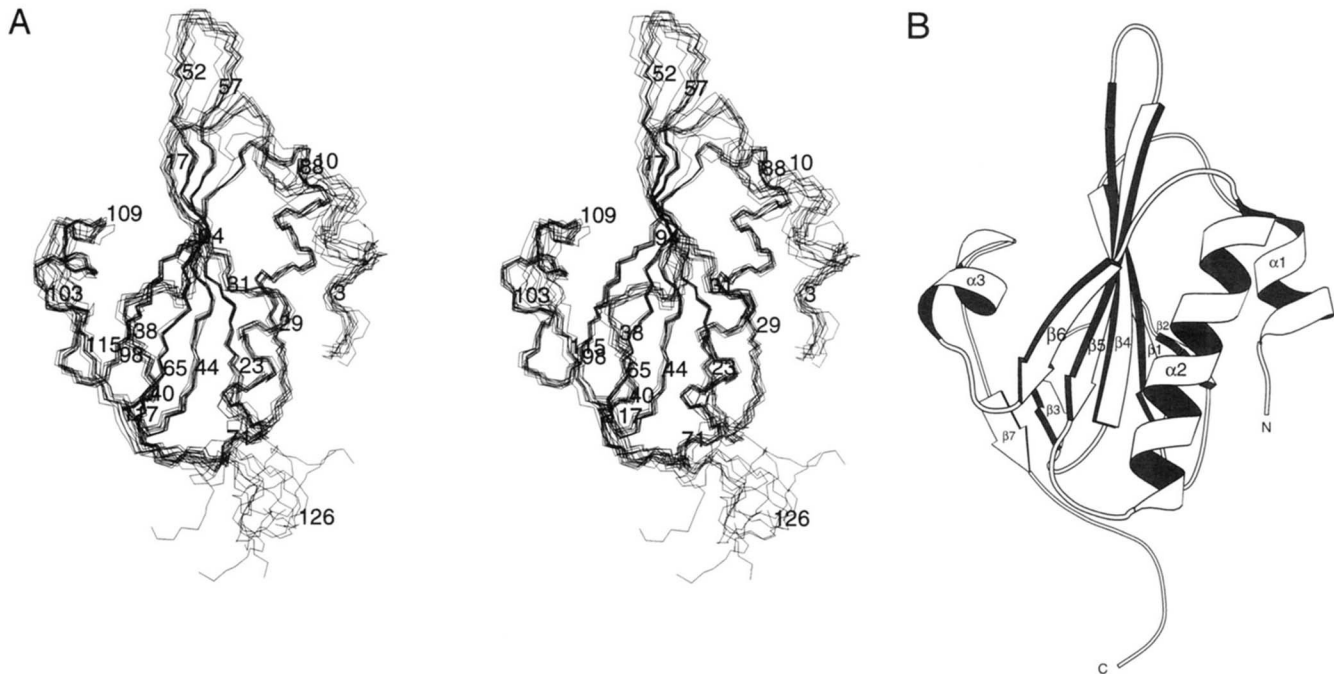


Fig. 1. **A:** Stereoview of the superimposed backbone atoms for 11 refined structures of villin 14T. For the alignment, residues 16–23, 29–31, 38–52, 57–110, and 114–118 were used. **B:** Ribbon diagram of villin 14T based on the structure with the lowest overall energy after the energy minimization in X-PLOR. The view is the same as in **A**. The elements of regular secondary structure are labeled. This figure was generated with the program MOLSCRIPT (Kraulis, 1991).

Table 2. Statistics from the X-PLOR energy minimization of the villin 14T structures

Acceptance criteria		
NOE violations above 0.5 Å	0	
Dihedral angle violations over 5°	0	
Accepted structures	11 out of 20	
Remaining violations		{DGr} ^a
NOE violations above 0.3 Å	0.45 ± 0.52	0
Dihedral angle violations over 3°	1.09 ± 0.54	2
NOE violations above 0.1 Å	16.55 ± 4.76	13
Dihedral angle violations over 1°	5.18 ± 2.09	5
RMSDs from idealized covalent geometry		
Bonds (Å)	0.00249 ± 0.00022	0.00216
Bond angles (°)	0.513 ± 0.020	0.479
Improper torsions (°)	0.383 ± 0.024	0.352
RMSDs from experimental constraints		
Distances (Å)	0.0229 ± 0.0029	0.0204
Dihedral angles (°)	0.576 ± 0.120	0.586
Final energies (kcal/mol)		
Overall	250 ± 29	204
Bonds	12.4 ± 2.2	9.32
Angles	143 ± 11	125
van der Waals	30.9 ± 6.8	17.9
Improper torsions	23.7 ± 3.0	20.0
Distance restraints	37.3 ± 9.8	29.2
Dihedral angle restraints	2.52 ± 1.01	2.51

^a{DGr} refers to the ensemble of 11 structures calculated with DG-II and energy minimized in X-PLOR 3.1. For the ensemble, the average plus or minus the standard deviation is quoted. {DGr}_r refers to the minimized average structure. The energy minimization essentially used the parallhdg.pro force field parameters supplied with X-PLOR 3.1, with repel set to 0.75, NOE force constants scaled by 50, and dihedral force constants scaled by 200.

Table 3. Pairwise RMSDs for different alignments of villin 14T structures

Description	Number of residues	{DGr} ^a versus {DGr} ^b		{DGr} versus {DGr} _r ^c		{DGr} versus {DG} ^d	
		Backbone	Heavy	Backbone	Heavy	Backbone	Heavy
Folded chain ^e	121	0.71 ± 0.11	1.07 ± 0.12	0.46	0.66	2.12 ± 0.15	2.83 ± 0.16
Elements of regular secondary structure ^f	72	0.58 ± 0.11	0.94 ± 0.13	0.37	0.62	1.50 ± 0.16	2.16 ± 0.16
Well-defined regions ^g	85	0.47 ± 0.12	0.87 ± 0.11	0.35	0.61	1.64 ± 0.17	2.35 ± 0.16

^a{DGr} indicates the set of 11 refined DG-II structures for villin 14T, presented here.

^b{DGr} indicates the average structure determined from the 11 refined DG-II structures.

^c{DGr}_r indicates the average structure determined from the 11 refined DG-II structures after energy minimization. Energy terms were added for experimental distance and dihedral angle restraints during minimization.

^d{DG} indicates the set of 10 DG-II structures for villin 14T, presented in Markus et al., 1994a.

^eResidues 1–121, omitting the carboxyl terminal tail (122–126), for which no medium or long range NOE crosspeaks were observed.

^fResidues 3–10, 17–23, 29–31, 38–40, 44–52, 57–65, 71–88, 94–98, 103–109, 115–117 (three helices and seven β -strands).

^gResidues 16–23, 29–31, 38–52, 57–110, 114–118 (regular secondary structure without the amino terminal helix but with some of the better-defined turns included).

above 0.1 Å is approximately 17 out of 1321. Violations of dihedral angle restraints were also small, with only one violation above 3° on average. The covalent geometry agrees well with the ideal values in the X-PLOR library. Before refinement, the energies for the structures calculated with DG-II were relatively high, with large contributions from the van der Waals term. However, restrained energy minimization in X-PLOR efficiently reduced all the energy terms to low values, as shown in Table 2.

Improved precision of the refined structure

The ensemble of structures in Figure 1A forms a tight bundle in regions of regular secondary structure when superimposed, with an $\langle \text{RMSD} \rangle$ of 0.58 ± 0.11 Å for the backbone atoms. The $\langle \text{RMSD} \rangle$ s for various calculated structures and superpositions are summarized in Table 3. Superposition of backbone atoms in residues 1–121 has an $\langle \text{RMSD} \rangle$ from the mean structure of 0.71 ± 0.11 Å compared to 1.15 ± 0.17 Å for the previously published structures. The pairwise RMSDs between the sets of structures for backbone atoms in residues 1–121 is 2.12 ± 0.15 Å. This value is within the sum of the pairwise RMSDs of the separate sets of structures ($\sqrt{2}$ times the RMSD to the mean structure), so in this sense, the old and the new structures agree to within their experimental precision.

The improved precision in the ensemble of refined structures is due to the increased number of NOE restraints. The distribution of those restraints per residue is shown in Figure 2A. Although the average number of NOE restraints per residue is relatively high (20.4 ± 15.9 , counting interresidue restraints twice, once for each residue), the variation is very great, from zero restraints for Asp¹² to 86 for Trp²¹. In general, residues with large side chains that participate in the hydrophobic core, like Trp²¹, have the most NOE restraints. Smaller side chains and residues that participate in turns between elements of secondary structure, like Asp¹², have the fewest NOE restraints. For villin 14T, the turns between elements of secondary structure are all on the surface of the molecule. In this position, the turn residues have fewer neighbors to exchange magnetization with during NOE experiments, so from geometrical considerations alone, they are expected to have fewer NOE restraints.

The effect of the distribution of the NOE restraints can be seen in the $\langle \text{RMSD} \rangle$ from the mean structure, plotted per residue in Figure 2B. In general, everywhere there is a dip in the number of restraints per residue, there is an increase in the $\langle \text{RMSD} \rangle$, and the

ensemble of structures shows less agreement. The most disorder is observed for residues in the turns between the elements of regular secondary structure. As already mentioned, the turn residues are at the surface of the molecule. Therefore, they potentially have more flexibility than residues in the core, with less packing to hold them rigid. Relaxation measurements for villin 14T (Markus et al., 1996),

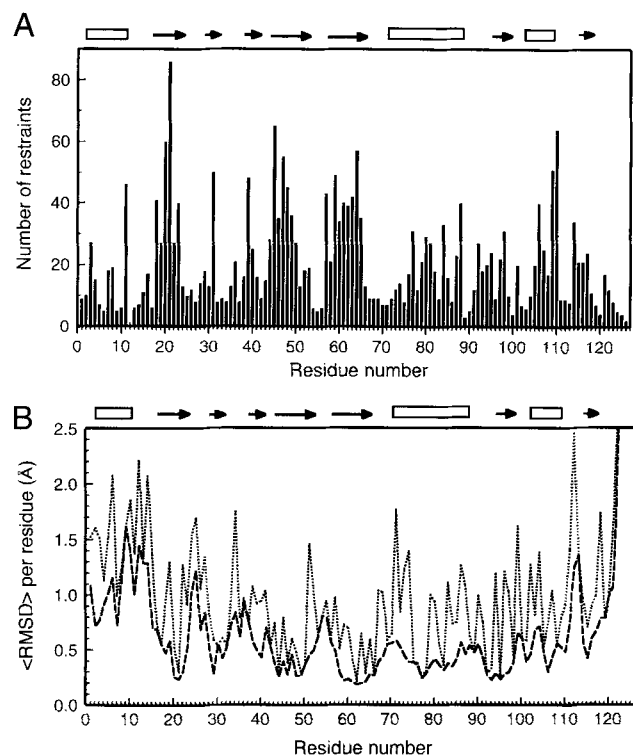


Fig. 2. **A:** Summary of the number of NOE restraints for each residue. Based on the list of 1,321 NOE restraints, the restraints per residue are tabulated. Restraints between two different residues are counted once for each residue. **B:** Plot of the average root-mean-square deviation ($\langle \text{RMSD} \rangle$) per residue for the 11 refined structures. The dashed line gives the $\langle \text{RMSD} \rangle$ as a function of sequence for the backbone atoms N, C_α, C', and O. The dotted line gives the $\langle \text{RMSD} \rangle$ for all heavy atoms in each residue. Above both panels, the secondary structure is shown schematically with rectangles representing helices and arrows representing strands of β -sheet.

which help discriminate between disorder due to the trivial lack of NOE restraints and disorder associated with mobility, suggest that some of the turns with relatively high RMSDs are more mobile. (The relaxation results will be reviewed in more detail in the Discussion section.) Also, Figure 2B reveals that helix $\alpha 1$ and the residues immediately following it are not particularly well defined. Side chains Lys⁵ and Lys⁶ in helix $\alpha 1$ have very similar chemical shifts, making assignment of their NOE crosspeaks difficult. Backbone amide crosspeaks could not be observed for residues Asp¹² and Lys¹³, which made it impossible to derive information for these residues from ¹⁵N-separated spectra. Relaxation measurements show that the amide proton of Leu¹¹ undergoes chemical exchange on a time scale of approximately 100 μ s (Markus et al., 1996), suggesting that the missing information in this region may be due, at least in part, to local conformational changes.

Precision of the dihedral angles

The Ramachandran plots for nonglycine residues in the refined villin 14T structures are shown in Supplementary Figure 1. In general, the backbone dihedral angles cluster in the preferred regions of (ϕ , ψ) space, with clusters near the ideal values for anti-parallel β -sheet (-139° , 135°), parallel β -sheet (-119° , 113°), and right-handed α -helix (-57° , -47°). However, as is often seen for NMR structures, there is some scatter into unfavored regions. When only residues with well-defined dihedral angles are considered, the scatter is greatly reduced (Suppl. Fig. 1B), suggesting that residues only appear to be in unfavored regions when they are ill defined. In that case, their calculated conformations reflect all the possible conformations consistent with the restraints. For the refined structures presented here, 84 residues have well-defined backbone dihedral angles, with angular order parameters over 90% (Hyberts et al., 1992). For the previously published structures, only 72 residues met this criterion. Therefore, despite the fact that no restraints were added for ϕ angles, the increase in the number of NOE restraints improved the definition of the backbone dihedral angles somewhat.

The average dihedral angles and their order parameters are shown in Supplementary Figure 2. Supplementary Figure 2A shows the average values of ϕ and ψ as a function of residue number. The elements of secondary structure are sketched above the panel; except for helix $\alpha 1$, which shows relatively low order parameters, the average backbone dihedral angles clearly map out the elements of secondary structure. Dips in the angular order parameters are observed between elements of secondary structure, especially between strands $\beta 1$ and $\beta 2$, $\beta 2$ and $\beta 3$, $\beta 3$ and $\beta 4$, helix $\alpha 2$ and strand $\beta 6$, strand $\beta 6$ and helix $\alpha 3$, and helix $\alpha 3$ and strand $\beta 7$, but not between strands $\beta 4$ and $\beta 5$ or between strand $\beta 5$ and helix $\alpha 2$. At this level of refinement, the tight β -turn between strands $\beta 4$ and $\beta 5$ can be classified as type III; the order parameters for the dihedral angles in the other tight turns, between strands $\beta 1$ and $\beta 2$ and at the end of strand $\beta 6$, are still too low for a meaningful classification. Ser⁷⁰, not Asn⁶⁸ as previously proposed, adopts the correct conformation to act as an N-cap to helix $\alpha 2$, with average values of -108° and 168° for ϕ and ψ and order parameters above 90%. Gly⁸⁹ acts as the C-cap for the same helix, with well-defined average angles of 105° and 21° for ϕ and ψ (Richardson & Richardson, 1988).

The average χ_1 side-chain angles and their order parameters are shown in Supplementary Figure 2B. The striking trend is for most of the angles to cluster about the expected rotamers at $+60^\circ$, 180° ,

and -60° . Dihedral angle restraints have been used in the calculations for only 53 of the 103 possible χ_1 angles, yet 62 angles have order parameters above 90%.

Definition of the side chains

Since many of the χ_1 dihedral angles are well defined, it seems reasonable to examine some of the side chains. The central β -sheet has hydrophobic patches on either side, which interact with hydrophobic side chains from helices $\alpha 1$ and $\alpha 2$ on one side and from helix $\alpha 3$ and the small parallel sheet on the other side. The side chains for residues in the β -sheet are shown in Figure 3. Side chains in the hydrophobic core are quite well defined, while side chains at the edges of the sheet and on the exposed surface of strands $\beta 4$ and $\beta 5$ (near residues 52 through 57) show more disorder. Therefore, at this level of refinement, the details of the orientation of the internal side chains become meaningful.

Discussion

How well does disorder in the ensemble of structures correlate with mobility?

The mobility of villin 14T has been probed on two time scales, approximately picosecond to nanosecond and microsecond to millisecond, using ¹⁵N and ¹H relaxation measurements (Markus et al., 1996). Although it is often implied that disordered regions in a set of calculated structures are more mobile, typically it is difficult to distinguish mobility from incomplete information, due to sources such as poor chemical shift dispersion, experimental artifacts, or unfavorable local geometry. For villin 14T, we can compare the relaxation at each residue with the $\langle \text{RMSD} \rangle$ and look for trends. The relaxation rate for the transverse component of the ¹⁵N magnetization is plotted as a function of residue for backbone amides in Figure 4. Regions with reduced relaxation rates are most likely undergoing motions on the picosecond-to-nanosecond time scale. Based on Figure 4, the turns between strands $\beta 3$ and $\beta 4$, $\beta 4$ and $\beta 5$, $\beta 6$ and helix $\alpha 3$, and helix $\alpha 3$ and strand $\beta 7$ show evidence of fast time-scale motion. Based on the $\langle \text{RMSD} \rangle$ per residue shown in Figure 2B, the $\langle \text{RMSD} \rangle$ for the backbone atoms is locally increased in these regions, but it is also increased in helix $\alpha 1$, between helix $\alpha 1$ and strand $\beta 1$, strands $\beta 1$ and $\beta 2$, $\beta 2$ and $\beta 3$, strand $\beta 5$ and helix $\alpha 2$, helix $\alpha 2$ and strand $\beta 6$. Evidence for mobility on the microsecond-to-millisecond time scale, based on $T_{1\rho}$ experiments, suggests mobility between helix $\alpha 1$ and strand $\beta 1$. However, there remain five regions with local increases in $\langle \text{RMSD} \rangle$ that do not correlate with relaxation evidence for mobility. It is possible that these regions display mobility on a time scale that is not readily probed by NMR experiments. It is also possible that local geometry limits the number of restraints available for these regions even when relatively artifact-free, completely assignable spectra are available, and thus limits the level of detail achievable for these regions.

Comparison with other actin-severing proteins

The refined structure of villin 14T is compared with the structures of gelsolin segment 1 and severin domain 2 in Figure 5. The structures were aligned first by superimposing regions with high sequence homology, then by superimposing residues that were close together in space. The sequences were realigned manually to

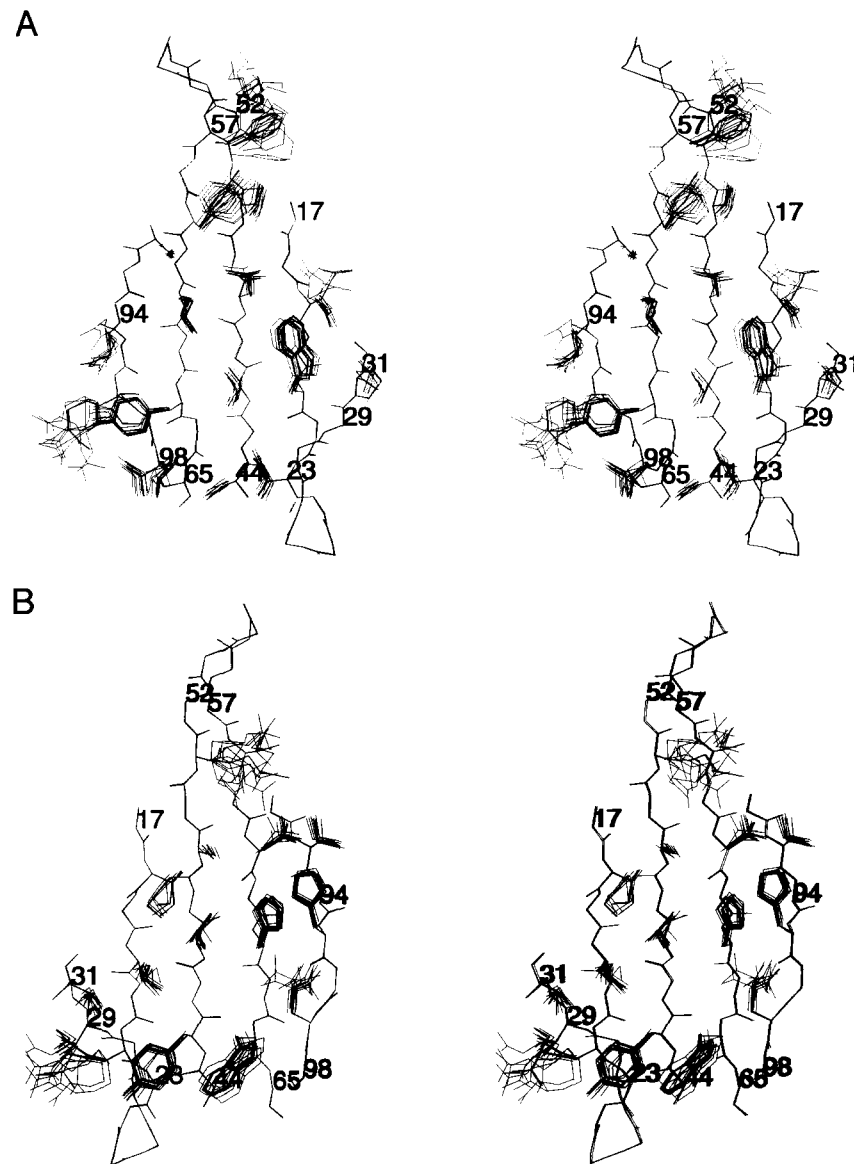


Fig. 3. Well-defined side chains in the hydrophobic core. **A:** Face of the central β -sheet covered by helices $\alpha 1$ and $\alpha 2$. **B:** Face of the central β -sheet covered by helix $\alpha 3$ and the small parallel sheet. Backbone atoms for one representative structure are shown together with side-chain atoms from all 11 refined structures. Endpoints of the elements of regular secondary structure are numbered. Although side chains at the edges of the sheet show some scatter, the side chains packed in the hydrophobic core of the villin 14T are well defined.

improve the correspondence between elements of secondary structure. Interestingly, the resulting alignment (Fig. 6) is very similar to the one obtained by Way and Weeds (1988) by considering sequence homologies in all the conserved domains from human gelsolin, pig gelsolin, villin, fragmin, and severin. Based on our alignment, backbone atoms for 50 out of 93 residues for severin domain 2, 120 residues for gelsolin segment 1, and 126 residues for villin 14T could be superimposed, with RMSDs of 1.07 Å between villin 14T and gelsolin segment 1, 1.97 Å between villin 14T and severin domain 2, and 1.87 Å between gelsolin segment 1 and severin domain 2. Villin 14T and gelsolin segment 1 (Figure 5A) correspond very closely, as might be expected from their 58% sequence identity. The largest changes are in strands $\beta 1$ and $\beta 2$, which turn away from the rest of the central β -sheet in gelsolin

segment 1, and in the orientation of helix $\alpha 3$. The longest strands of the β -sheet, strands $\beta 4$ and $\beta 5$, and the parallel edge strand $\beta 6$, as well as helix $\alpha 2$, the site for actin binding, have nearly identical backbone orientations. Severin segment 2, with only 20% sequence identity to villin 14T, shows more differences. The fragment of severin domain 2 constructed for structural studies is similar in size to villin 14T. However, the region for which the structure is reported is shorter. The pieces of severin domain 2 corresponding to helix $\alpha 1$ and strand $\beta 7$ in villin 14T are apparently unstructured in solution (Schnuchel et al., 1995). Comparing the remaining pieces (Fig. 5B), strands $\beta 1$ and $\beta 2$ are longer in severin domain 2, causing the turn between them to project further into the surrounding solvent. Strands $\beta 4$ and $\beta 5$ are much shorter in severin domain 2, eliminating the flexible loop observed in

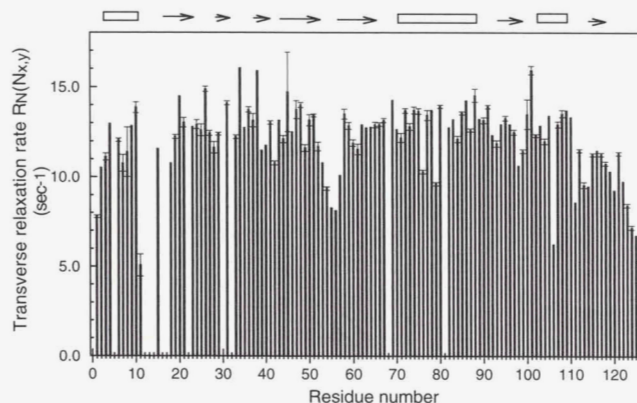


Fig. 4. Relaxation rate for transverse nitrogen magnetization for backbone amides in villin 14T. Large values typically reflect exchange contributions which imply mobility on the millisecond time scale. Small values typically reflect increased values of the spectral density at high frequencies, implying motions on the picosecond to nanosecond time scale.

villin 14T. However, as in the comparison with gelsolin segment 1, the remainder of strands $\beta 4$ and $\beta 5$, strand $\beta 6$, and even helix $\alpha 2$ superimpose quite closely.

The details of the structural similarity among villin 14T, gelsolin segment 1, and severin domain 2 are brought out by the sequence comparison in Figure 6. The hydrophobic core of the domain is well conserved, as can be seen from the residues colored blue. The hydrophobic residues are not identically conserved—conservative substitutions including isoleucine for leucine, leucine for phenylalanine or tyrosine, and phenylalanine for tryptophan have been included among the blue residues. This suggests that the hydrophobic packing is not very specific and can adjust to changes in the details but not the character of the side chains. The residues that promote turns between the elements of secondary structure are very well conserved, shown by the glycine and proline residues in green in Figure 6. For this domain, each β -strand and α -helix is oriented almost 180° from the previous element of secondary structure, forming sharp turns near the surface at every connection. To

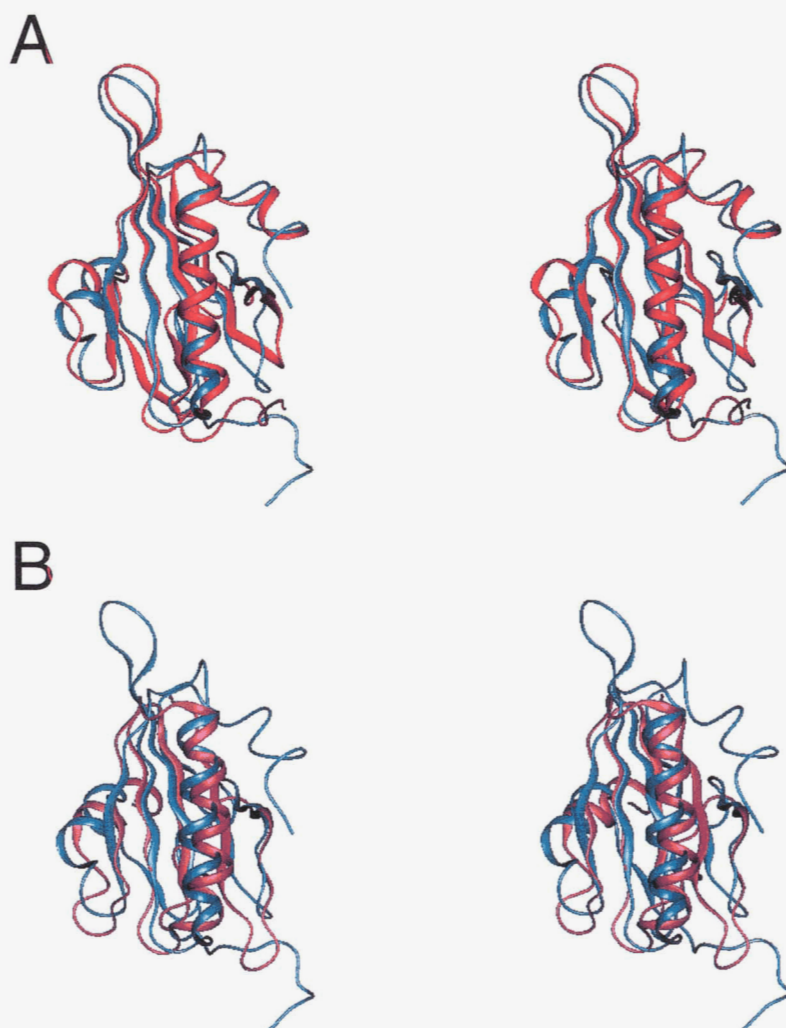


Fig. 5. Pairwise comparison of domains from the actin severing family. **A:** Villin 14T (blue) and gelsolin segment 1 (red). **B:** Villin 14T (blue) and severin domain 2 (violet). The structures are rotated compared to Fig. 1 so that helix $\alpha 2$, which is the center for hydrophobic interactions with actin, is in front. The structures are presented as stereopairs of ribbon diagrams, generated with Quanta (Molecular Simulations, Inc., Burlington, Massachusetts). Coordinates for severin domain 2 were obtained from the Brookhaven Protein Data Bank (entry 1SVQ; Schnuchel et al., 1995).

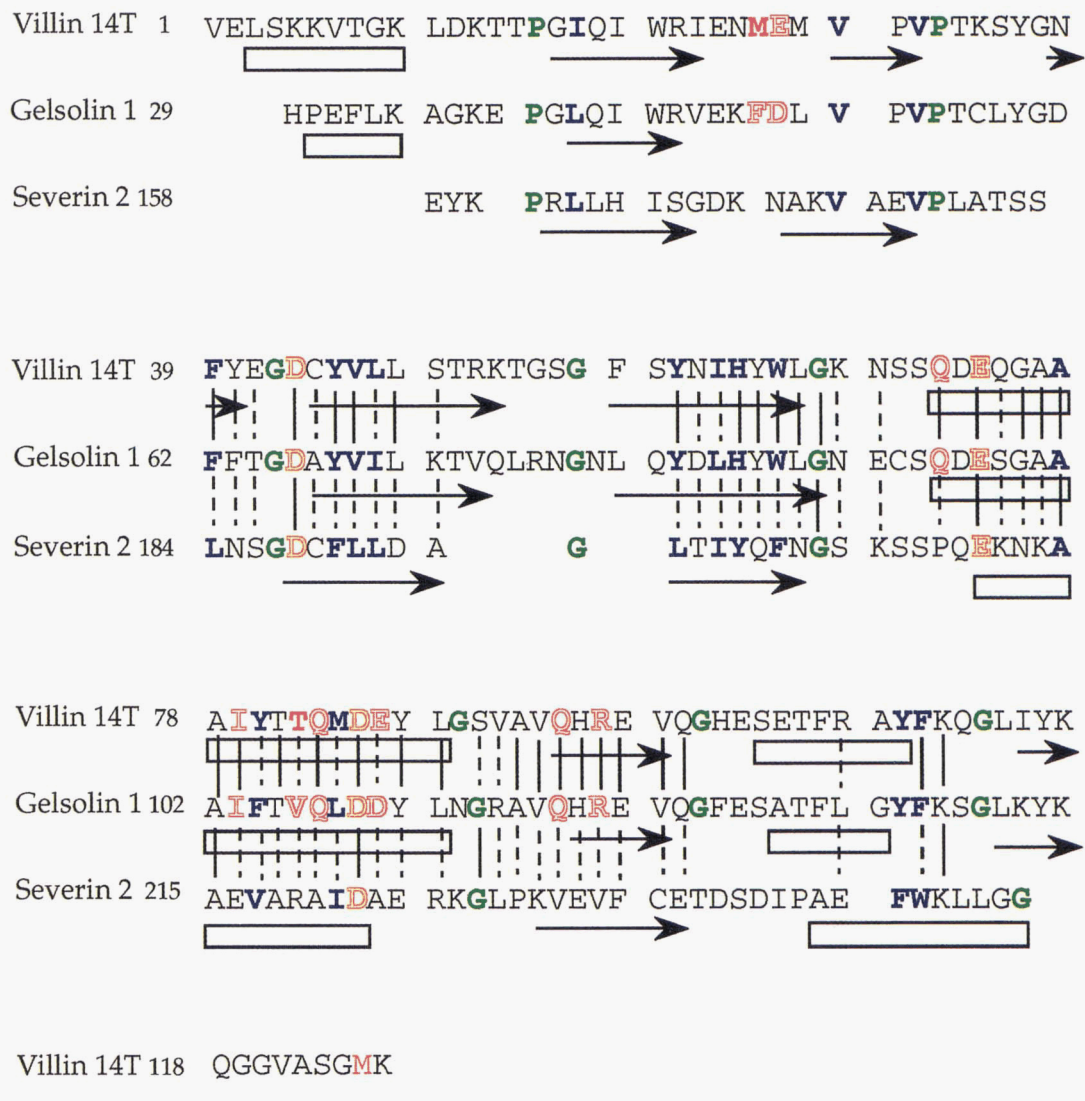


Fig. 6. Comparison of the amino acid sequences for villin 14T, gelsolin segment 1, and severin domain 2. The amino acids are represented by the one-letter code. Sequence numbers are indicated on the left. Elements of secondary structure are indicated below the amino acid sequence, with open rectangles representing α -helices and arrows representing strands of β -sheet. The sequences were aligned first by sequence and then by secondary structure, with manual adjustments to improve the alignment of elements of secondary structure. Aligned residues used to superimpose the structures in Fig. 5 are denoted by connecting lines; solid lines indicate sequence identity and dashed lines indicate different residues in similar locations. Residues are color-coded by function. Side chains that correspond to the hydrophobic core in villin 14T and which are conserved in the other domains are shown in blue. The glycines and prolines important for delineating elements of secondary structure are shown in green. Side chains that provide calcium ligands, based on the structure of gelsolin segment 1 in a co-crystal with actin (McLaughlin et al., 1993), are shown in gold outlined letters. Notice that these residues are strictly conserved in all three domains. Side chains that interact with actin, based on the gelsolin segment 1 co-crystal with actin, are shown in red outlined letters. Notice that severin domain 2, which does not show ability to bind to actin, has non-conserved residues in these locations, while villin 14T, which requires higher calcium concentrations than gelsolin segment 1 to bind actin monomers, has identical residues in most of the positions and a few conservative replacements (solid red letters).

make these sharp turns, the small glycine residues are probably particularly important. Finally, the calcium binding residues, as identified in the gelsolin segment 1 co-crystal with actin, are shown in orange outlined letters in Figure 6. These residues are perfectly conserved and aligned among these three representative domains.

Villin 14T and gelsolin segment 1 both bind to actin monomers, while severin domain 2 is thought to bind along actin filaments.

Examination of the residues important for binding actin monomers brings out the differences between villin 14T and gelsolin segment 1. The residues important for actin binding, based on the structure of the gelsolin segment 1–actin complex (McLaughlin et al., 1993), are shown in red in Figure 6. Gelsolin segment 1 presents actin with a patch of hydrophobic residues centered on Ile¹⁰³ (which corresponds to Ile⁷⁹ in villin 14T) rimmed with

hydrogen bond donors. Residues corresponding to Gln⁹⁴ and Arg⁹⁶ in strand β 6 are involved in hydrogen bonds, as are Glu²⁷, Tyr⁵⁹, Gln⁷¹, Gln⁸³, and Glu⁸⁶. These residues are conserved between villin 14T and gelsolin segment 1; the amino acid types agree except for Glu²⁷ and Glu⁸⁶, which are conservative replacements for Asp⁵⁰ and Asp¹¹⁰ in gelsolin. Comparison of the hydrophobic residues available for the interaction in villin 14T versus gelsolin segment 1 suggests a possible reason for villin 14T's lower affinity for actin. In the complex with actin, gelsolin residues Phe⁴⁹, Ile¹⁰³, Val¹⁰⁶, and Phe¹⁴⁹ contribute to the apolar actin-binding surface. In villin 14T, the isoleucine is conserved but the other side chains are replaced with somewhat smaller, less hydrophobic counterparts (Met²⁶, Thr⁸², and Met¹²⁵). In striking contrast, none of these residues are conserved in the actin filament binding domain, severin domain 2.

A further look at the surfaces presented by villin 14T and by gelsolin segment 1 to actin monomers reveals another difference. Despite the fact that the side chains on the surface of villin 14T are not precisely defined even at this level of refinement, the overall surface features near Ile⁷⁹ in villin 14T and Ile¹⁰³ in gelsolin segment 1 are very similar (compare regions near the asterisks in Fig. 7A, B). For both villin 14T and gelsolin segment 1, this isoleucine contributes to a local ridge, but severin domain 2 has a local depression flanked by protruding positive side chains at the corresponding position (Fig. 7C). The charge distributions are more neutral in the actin monomer-binding domains from villin and gelsolin, except for a more negative patch in the turn between strands β 1 and β 2 for villin 14T (lower right in Fig. 7A) compared to gelsolin (Fig. 7B). Villin 14T and gelsolin segment 1 both have two negatively charged side chains in this turn, Glu²⁴ and Glu²⁷ in villin 14T and Glu⁴⁷ and Asp⁵⁰ in gelsolin segment 1. In gelsolin segment 1, these negative charges are partially offset by Lys³⁸, which is replaced by Asn²⁵ in villin 14T. Note that this site is very close to Phe⁴⁹ in gelsolin segment 1, part of the hydrophobic patch for actin monomer binding. It is also close to the intramolecular calcium binding site. Villin 14T may require higher calcium concentrations for actin monomer binding to compensate for this negative charge, although titration experiments monitored by NMR only detected one binding site in this region (Markus et al., 1994a).

With knowledge of the structures of villin 14T and severin domain 2, which has 43% sequence identity to villin domain 2, it is tempting to speculate on the structure of a two-domain piece, and therefore predict the structure of a molecule with severing activity. However, about 10 amino acids link the last well-defined residue in villin 14T (Val¹²¹) with the first position reported for severin domain 2. This 10-amino acid linker is long enough to traverse the longest dimension of the domain and it is difficult to speculate how the domains will pack together. The structure of a two or more domain piece remains a challenge for future structural studies.

Models for severing

On the basis of biochemical data for gelsolin, the general features of a mechanism for actin severing and capping have been proposed (Pope et al., 1991; Way et al., 1992). Domain 2, which contains an actin-filament binding site, targets the severing protein to the actin filament. Then, domain 1 binds to a nearby actin monomer and disrupts interactions between monomers in the filament. The severing protein then remains bound to the barbed end of the filament, creating a cap that prevents elongation. With the crystal structure of the gelsolin segment 1–actin complex (McLaughlin et al., 1993)

and a model for the actin filament (Holmes et al., 1990), McLaughlin et al. (1993) propose a more detailed mechanism for filament disruption. They suggest that the first domain of gelsolin (segment 1), as bound to actin in the crystal, would disrupt interactions between actin monomers within one strand of the two-start helix. Specifically, the gelsolin segment 1 bound between subdomains 1 and 3 of one actin monomer would disrupt packing against subdomain 2 of the next. This model would require only a glancing interaction with the actin filament, which should be energetically more favorable than an insertion that competes with the entire actin–actin contact site. Yet this glancing interaction would disrupt the actin–actin contacts along one strand, which are proposed to be the stronger interactions in the filament (Holmes et al., 1990).

McLaughlin et al. (1993) go on to propose a model for arranging all six domains of gelsolin around the actin filament. The model then features domains 1 and 4 bound to actin monomers in each strand of the two-start helix within the filament, with domains 2 and 3 strung in between, across the filament in the orientation that covers the shorter distance (see Fig. 8A).

Way and Matsudaira suggest an alternative model for gelsolin binding to the actin filament (Way & Matsudaira, 1993; sketched in Fig. 8B). Their model is based on evidence that the α -actinin filament binding site can functionally replace the domain 2 site (Way et al., 1992) and that α -actinin binds along strands of the two-start helix in actin filaments (McGough et al., 1994). Way and Matsudaira suggest that the second domain of gelsolin should bind along, not across, the actin filament axis. A three-dimensional model corresponding to the along-the-strand model (McGough & Way, 1995) has been constructed from information from the gelsolin–actin co-crystal structure, the villin 14T structure, the model of the actin filament (Holmes et al., 1990), and electron microscopy studies of α -actinin bound to actin filaments.

A drawback of the across-the-strand model is that it assumes gelsolin is in the correct orientation to nucleate, sever, and cap filaments all at the same time. Since nucleating filament growth and capping filament growth seem to be incompatible activities, this assumption may not be correct. Noting that domains 2–6 can nucleate filament growth and that domains 1–3 have nearly full severing activity, it may be that these functions involve the interaction of only two actin-binding sites at a time. The activity observed, and the actin-binding sites occupied, would be determined by the relative concentrations of actin monomers and filaments and regulatory molecules such as calcium ions and polyphosphoinositides.

For an understanding of function in terms of structure, it is important to examine an appropriate model system. The co-crystal of gelsolin segment 1 with actin is a good model for the domain 1–actin monomer interaction. Biochemical studies have suggested that this interaction disrupts actin–actin contacts in filaments. Therefore, the structure of the complex, taken with the model of the actin filament, offers immediate insight into the atomic details of this step in the severing process. However, attempts to extend the model to include the missing domains only lead to more questions.

Comparison with the actin-regulating protein destrin

The solution structure of destrin shows that it adopts the same overall fold as the actin-severing domains (Hatanaka et al., 1996, especially Fig. 3). Destrin, and the closely related cofilin proteins, bind to actin monomer and filaments and sever actin filaments all with a single domain. Thus destrin, or some member of the cofilin

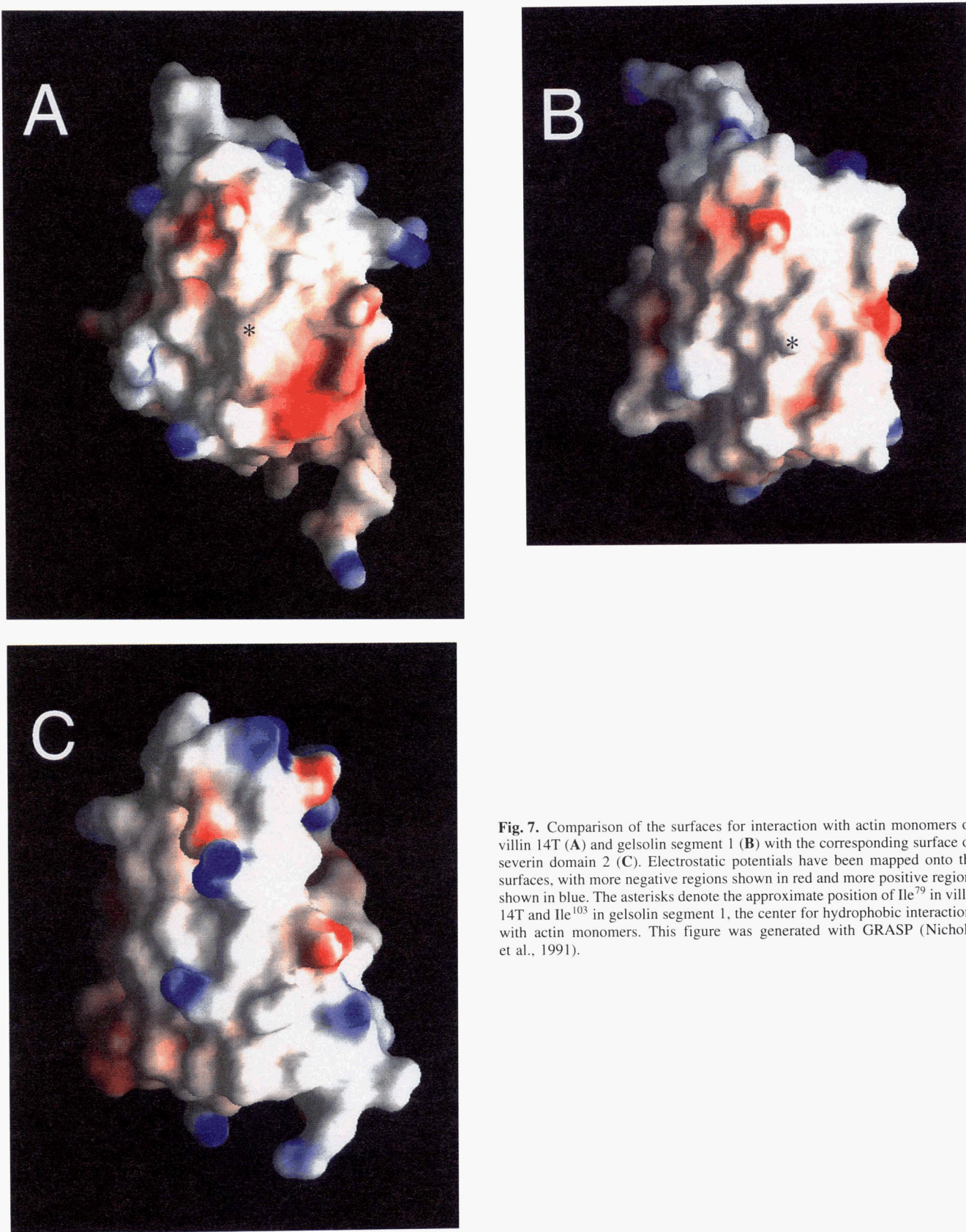


Fig. 7. Comparison of the surfaces for interaction with actin monomers on villin 14T (**A**) and gelsolin segment 1 (**B**) with the corresponding surface on severin domain 2 (**C**). Electrostatic potentials have been mapped onto the surfaces, with more negative regions shown in red and more positive regions shown in blue. The asterisks denote the approximate position of Ile⁷⁹ in villin 14T and Ile¹⁰³ in gelsolin segment 1, the center for hydrophobic interactions with actin monomers. This figure was generated with GRASP (Nicholls et al., 1991).

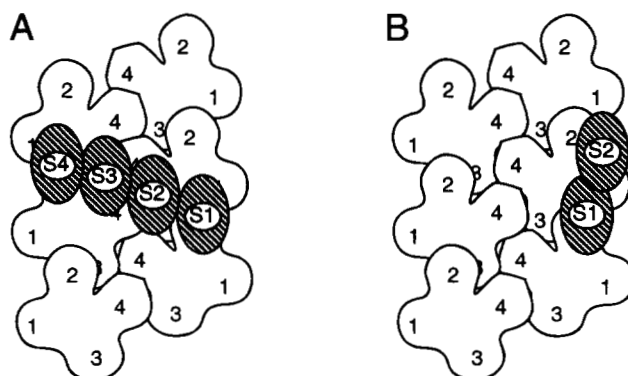


Fig. 8. Contrasting models for gelsolin binding to actin filaments. **A:** The domains of gelsolin continue from segment 1 across the actin filament axis (McLaughlin et al., 1993). **B:** Domain 2 of gelsolin continues along the filament axis (Way & Matsudaira, 1993). Actin is represented by the four-lobed shapes. The subdomains of the actin monomer are numbered 1–4. Structural domains of gelsolin are represented by hatched ovals. The domains are numbered S1–S4. The barbed end of the actin filament, associated with rapid monomer addition, is at the bottom of the figure; the pointed end is at the top. (This figure is adapted from Fig. 3 in Way & Matsudaira, 1993.)

family, is a possible source for the single-domain gene that was duplicated to form the multi-domain actin-severing proteins (Hofmann et al., 1993). Comparison of the sequences of destrin and villin 14T, aligned by structural elements (Hatanaka et al., 1996) and allowing conservative replacements in the sets (R, K), (V, I, L, F, Y, W, H), and (E, Q), shows that the sequence similarity is about 21%, consistent with the similarity in the fold. Two of the proposed calcium binding ligands for villin 14T are not conserved in destrin, consistent with destrin's calcium-independent affinity for actin. However, since the sequence identity between destrin and villin 14T is low (almost 9%), any proposed gene duplication must have occurred long ago in evolution. The details of the putative evolutionary relationship between the actin-severing proteins and the cofilins will require further analysis of more protein sequences.

Conclusions

Comparison of the structures for villin 14T, gelsolin segment 1, and severin domain 2, brings out the important features of the conserved fold for the actin-severing proteins. The distribution of conserved hydrophobic residues, important for packing the core, and conserved glycine and proline residues, which participate in key turns dividing the elements of regular secondary structure, establish the fold for the domain. Calcium-binding ligands are also strongly conserved. Non-conserved sequences, primarily along the surface-exposed edge of the central β -sheet, the parallel β -sheet, and helix α 3, determine whether an individual domain will interact with actin monomers. As more structures are solved, it will be interesting to see how the domains interact with each other and the details of regulation by polyphosphoinositides.

Materials and methods

Protein samples for solution NMR studies

Villin 14T includes the 126 amino-terminal residues from the chicken epithelial sequence of the protein villin. The expression in *Esch-*

erichia coli and purification have been described (Markus et al., 1994b). Samples labeled with ^{15}N alone, both ^{13}C and ^{15}N , and ^{13}C to 10% as well as unlabeled samples were prepared. The sample buffer for structure determination is 50 mM NaH_2PO_4 , pH 4.15, 100 mM NaCl, and 0.1 mM NaN_3 . Sample concentrations ranged from 1.65 to 6.72 mM.

NMR data collection and processing

The NMR experiments have been described in detail (Markus et al., 1994b). Briefly, NMR measurements were performed on AMX500 and AMX600 spectrometers (Bruker, Karlsruhe, Germany) at 25 °C. Data were processed using the Felix software package (formerly Hare Research Inc., Bothell, Washington; more recently Biosym Technologies, San Diego, California). The HNCA and HN(CO)CA pair of experiments was used for sequential assignments (Kay et al., 1990; Bax & Ikura, 1991; Grzesiek & Bax, 1992). The sequential assignments were confirmed with the HNCO (Grzesiek & Bax, 1992) and HCACO (Powers et al., 1991) pair of experiments. For side-chain assignments, experiments included ^{15}N -dispersed TOCSY (Marion et al., 1989a) and a ^{13}C heteronuclear crosspolarization experiment (HEHOHEHAHA, Majumdar et al., 1993) as well as conventional 2D TOCSY (Braunschweiler & Ernst, 1983) and double quantum filtered COSY (Piantini et al., 1982).

After the initial assignments and structure determination, another ^{15}N -dispersed NOESY was acquired with a shorter mixing time. The sequence used an HSQC module to improve resolution in the ^{15}N dimension (Bax et al., 1990) and gradient water suppression (Kay et al., 1993). The spectrum was recorded on a ^{15}N -labeled sample at 2.29 mM, with a mixing time of 80 ms and sign discrimination by States-TPPI in both indirect dimensions. The spectral widths were 14.08 ppm in $\text{F}_1(^1\text{H})$, 45.0 ppm in $\text{F}_2(^{15}\text{N})$, and 14.08 ppm in $\text{F}_3(^1\text{H})$, with 152 complex by 47 complex by 512 complex points and eight scans per increment. The carrier for ^{15}N was set to 123.0 ppm. Note that even though this spectrum used a shorter mixing time than the original ^{15}N NOESY HMQC, due to the improved pulse sequence and better resolution in the indirect proton dimension, more peaks could be assigned.

NOE restraints

NOE restraints were based on experiments including 3D ^{15}N - and ^{13}C -dispersed NOESY (Marion et al., 1989a, 1989b) in addition to 2D NOESY in H_2O and D_2O . The spectra were recorded with mixing times of 80, 100, and 150 milliseconds, and crosspeaks were only loosely quantified by counting plotted contour levels. Crosspeak intensity was correlated with distance by examining the intensity of crosspeaks between backbone protons involved in regular secondary structure and assuming regular geometries. Peaks were then classified as strong, with an associated upper distance limit of 3.0 Å, intermediate, with a limit of 4.0 Å, and weak, with a limit of 5.0 Å. The difference between the number of assigned NOE crosspeaks and the number of distance restraints for structure calculation reported in Table 1 is due to methylene protons that lack stereospecific assignments.

Early in the structure determination, NOE crosspeak assignments were based on chemical shifts alone. To avoid ambiguities, attention focused on the 3D ^{15}N - and ^{13}C -dispersed data sets. The ^{15}N dispersed data sets proved to be easier to assign, due to more complete ^{15}N assignments, less overlap in the ^{15}N chemical shifts,

and fewer artifacts in the spectra. The 2D data sets were also used at an early stage, but attention focused on unique chemical shifts, as for the aromatic ring systems and methyl groups. As NOE crosspeaks were assigned, a physical model of the structure was built. This model was used as a reference to identify improbable assignments and in some cases to eliminate enough alternatives to decide on otherwise ambiguous assignments.

After publication of the "low-to-medium" precision distance geometry structure, that structure was used in conjunction with a FORTRAN program written by Sekhar Talluri (unpubl. results) to assist in the assignments. The program requires a reference set of pdb-format structures and lists of the assignments. When supplied with the chemical shifts of an unassigned peak, the program identifies all protons within a specified chemical shift tolerance and within a specified distance cutoff. This program greatly increased the speed of assignments.

Restraints on the dihedral angles and stereospecific assignments

The α -proton to amide proton scalar coupling constant ($^3J_{\text{HNH}\alpha}$) was determined from crosspeak splitting in the proton dimension of an ^{15}N heteronuclear correlation spectrum and confirmed with data from the HNHA experiment (Vuister & Bax, 1993). The backbone torsion angle ϕ was then restrained to the range -90° to -40° for $^3J_{\text{HNH}\alpha}$ less than or equal to 5.5 Hz and -160° to -80° for $^3J_{\text{HNH}\alpha}$ greater than 8.0 Hz. The side-chain torsion angle χ_1 was restrained based on two coupling constants. The α proton to β proton coupling constant ($^3J_{\text{H}\alpha\text{H}\beta}$) was classified as large or small from the COSY data; this result was compared to the qualitative measure based on intraresidue HN-H β crosspeak intensities in an ^{15}N dispersed TOCSY with a short spin lock (Clore et al., 1991). The amide nitrogen to β proton coupling constant ($^3J_{\text{NH}\beta}$) was classified as large or small from the HNHB experiment (Archer et al., 1991). Stereospecific assignments for methyl groups of valine and leucine were obtained from spectra acquired on the 10% ^{13}C -labeled sample (Neri et al., 1989; Senn et al., 1989; Szyperski et al., 1992).

Hydrogen bond restraints

The hydrogen bonds were assigned for regions of regular secondary structure based on hydrogen exchange data (Markus et al., 1994b) and characteristic NOE patterns. For each hydrogen bond, there are two restraints to maintain a somewhat linear bond geometry.

Structure calculations

To calculate the structure, the distance geometry algorithm implemented in the program DG-II (Havel, 1991) was used as part of the INSIGHT II software package (Biosym Technologies, San Diego, California). For the optimization step of DG-II, an initial energy of 4,500 kcal/mol with a time step of 0.38 ps gave convergence for 18 out of 20 structures to a final DG error of less than 1.00. These structures were subjected to 3,000 steps of Powell minimization in X-PLOR (Brünger, 1992) using an energy function including bond, angle, improper torsion, and van der Waals terms as well as terms to enforce NOE and dihedral angle restraints. After minimization, 11 of the 18 structures had no NOE violations over 0.5 Å and no dihedral angle violations over 5° and were accepted for further analysis. These 11 structures have an average overall energy of 250 ± 29 kcal/mol.

The coordinates for the 11 structures described here have been deposited in the Brookhaven Protein Data Bank as entry 2VIL. The minimized average structure is available as 2VIK.

Supplementary material in Electronic Appendix

Supplementary Figure 1, showing the Ramachandran plots, and Supplementary Figure 2, showing the average backbone and χ_1 dihedral angles with order parameters, are available in the Electronic Appendix.

Acknowledgments

This work was supported by NIH grant GM38608 (G.W.) and grant DK35306 (P.M.). Computer facilities used for the structure calculations were funded in part by the W.M. Keck Foundation. We thank Paul McLaughlin for the coordinates for gelsolin segment 1, based on the co-crystal structure with actin. We thank Peter Schmidt, George Planansky, and Timothy Havel for long-distance computer support. We thank Daniel Wyss, Jane Withka, Sven Hyberts, and Sekhar Talluri for advice on energy refinement of NMR-derived protein structures and for useful computer programs. M.A.M. thanks Dennis Torchia for the opportunity to finish this work.

References

- Archer SJ, Ikura M, Torchia DA, Bax A. 1991. An alternative 3D NMR technique for correlating backbone ^{15}N with side chain H β resonances in larger proteins. *J Magn Reson* 95:636–641.
- Arpin M, Pringault E, Finidori J, Garcia A, Jeltsch J-M, Vandekerckhove J, Louvard D. 1988. Sequence of human villin: A large duplicated domain homologous with other actin-severing proteins and a unique small carboxy-terminal domain related to villin specificity. *J Cell Biol* 107:1759–1766.
- Bax A, Ikura M, Kay LE, Torchia DA, Tschudin R. 1990. Comparison of different modes of two-dimensional reverse correlation NMR for the study of proteins. *J Magn Reson* 86:304–318.
- Bax A, Ikura M. 1991. An efficient 3D NMR technique for correlating the proton and ^{15}N backbone amide resonances with the α -carbon of the preceding residue in uniformly $^{15}\text{N}/^{13}\text{C}$ enriched proteins. *J Biomol NMR* 1:99–104.
- Bazari WL, Matsudaira P, Wallek M, Smeal T, Jakes R, Ahmed Y. 1988. Villin sequence and peptide map identify six homologous domains. *Proc Natl Acad USA* 85:4986–4990.
- Braunschweiler L, Ernst RR. 1983. Coherence transfer by isotropic mixing: Application to proton correlation spectroscopy. *J Magn Reson* 53:521–528.
- Brünger A. 1992. *X-PLOR Version 3.1. A system for crystallography and NMR*. New Haven, Connecticut: Yale University Press.
- Bryan J. 1988. Gelsolin has three actin-binding sites. *J Cell Biol* 106:1553–1562.
- Clore GM, Bax A, Gronenborn AM. 1991. Stereospecific assignment of β -methylene protons in larger proteins using 3D ^{15}N -separated Hartmann-Hahn and ^{13}C -separated rotating frame Overhauser spectroscopy. *J Biomol NMR* 1:13–22.
- Finidori J, Friederich E, Kwiatkowski DJ, Louvard D. 1992. In vivo analysis of functional domains from villin and gelsolin. *J Cell Biol* 116:1145–1155.
- Grzesiek S, Bax A. 1992. Improved 3D triple-resonance NMR techniques applied to a 31 kDa protein. *J Magn Reson* 96:432–440.
- Hatanaka H, Ogura K, Moriyama K, Ichikawa S, Yahara I, Inagaki F. 1996. Tertiary structure of destinin and structural similarity between two actin-regulating protein families. *Cell* 85:1047–1055.
- Havel TF. 1991. An evaluation of computational strategies for use in the determination of protein structure from distance constraints obtained by nuclear magnetic resonance. *Prog Biophys Mol Biol* 56:43–78.
- Hofmann A, Noegel AA, Bomblies L, Lottspeich F, Schleicher M. 1993. The 100 kDa F-actin capping protein of *Dictyostelium* amoebae is a villin prototype ("protovillin"). *FEBS Lett* 328:71–76.
- Holmes KC, Popp D, Gebhard W, Kabsch W. 1990. Atomic model of the actin filament. *Nature* 347:44–49.
- Hyberts SG, Goldberg MS, Havel TF, Wagner G. 1992. The solution structure of eglin c based on measurements of many NOEs and coupling constants and its comparison with X-ray structures. *Protein Sci* 1:736–751.
- Janmey PA, Matsudaira PT. 1988. Functional comparison of villin and gelsolin: Effects of Ca^{2+} , KCl, and polyphosphoinositides. *J Biol Chem* 263:16738–16743.

- Kabsch W, Sander C. 1983. Dictionary of protein secondary structure: Pattern recognition of hydrogen-bonded and geometrical features. *Biopolymers* 22:2577–2637.
- Kay LE, Ikura M, Tschudin R, Bax A. 1990. Three-dimensional triple-resonance NMR spectroscopy of isotopically enriched proteins. *J Magn Reson* 89:496–514.
- Kay LE, Xu G, Singer AU, Muhandiram DR, Forman-Kay, JD. 1993. A gradient-enhanced HCCH-TOCSY experiment for recording side-chain ^1H and ^{13}C correlations in H_2O samples of proteins. *J Magn Reson B* 101:333–337.
- Kraulis P. 1991. MOLSCRIPT: A program to produce both detailed and schematic plots of protein structures. *J Appl Cryst* 24:946–950.
- Kwiatkowski DJ, Janmey PA, Mole JE, Yin HL. 1985. Isolation and properties of two actin-binding domains in gelsolin. *J Biol Chem* 260:15232–15238.
- Kwiatkowski DJ, Janmey PA, Yin HL. 1989. Identification of critical functional and regulatory domains in gelsolin. *J Cell Biol* 108:1717–1726.
- MacArthur MW, Thornton JM. 1993. Conformational analysis of protein structures derived from NMR data. *Proteins Struct Funct Gen* 17:232–251.
- Majumdar A, Wang H, Morshauser RC, Zuiderweg ERP. 1993. Sensitivity improvement in 2D and 3D HCCH spectroscopy using heteronuclear cross-polarization. *J Biomol NMR* 3:387–397.
- Marion D, Driscoll PC, Kay LE, Wingfield PT, Bax A, Gronenborn AM, Clore GM. 1989a. Overcoming the overlap problem in the assignment of ^1H NMR spectra of larger proteins by use of three-dimensional heteronuclear ^1H - ^{15}N Hartmann-Hahn-multiple quantum coherence and nuclear Overhauser-multiple quantum coherence spectroscopy: Application to interleukin 1 β . *Biochemistry* 28:6150–6156.
- Marion D, Kay LE, Sparks SW, Torchia DA, Bax A. 1989b. Three-dimensional heteronuclear NMR of ^{15}N -labeled proteins. *J Am Chem Soc* 111:1515–1517.
- Markus MA, Dayic KT, Matsudaira P, Wagner G. 1996. Local mobility within villin 14T probed via heteronuclear relaxation measurements and a reduced spectral density mapping. *Biochemistry* 35:1722–1732.
- Markus MA, Nakayama T, Matsudaira P, Wagner G. 1994a. Solution structure of villin 14T, a domain conserved among actin-severing proteins. *Protein Sci* 3:70–81.
- Markus MA, Nakayama T, Matsudaira P, Wagner G. 1994b. Assignments for villin 14T, a domain conserved among actin-severing proteins. *J Biomol NMR* 4:553–574.
- Matsudaira P, Janmey P. 1988. Pieces in the actin-severing protein puzzle. *Cell* 54:139–140.
- McGough A, Way M. 1995. Molecular model of an actin filament capped by a severing protein. *J Struct Biol* 115:144–150.
- McGough A, Way M, DeRosier D. 1994. Determination of the α -actinin-binding site on actin filaments by cryoelectron microscopy and image analysis. *J Cell Biol* 126:433–443.
- McLaughlin PJ, Gooch JT, Mannherz HG, Weeds AG. 1993. Structure of gelsolin segment 1-actin complex and the mechanism of filament severing. *Nature* 364:685–692.
- Neri D, Szyperski T, Otting G, Senn H, Wüthrich K. 1989. Stereospecific nuclear magnetic resonance assignments of the methyl groups of valine and leucine in the DNA-binding domain of the 434 repressor by biosynthetically directed fractional ^{13}C labeling. *Biochemistry* 28:7510–7516.
- Nicholls A, Sharp KA, Honig B. 1991. Protein folding and association: Insights from the interfacial and thermodynamic properties of hydrocarbons. *Proteins Struct Funct Gen* 11:281–296.
- Piantini U, Sørensen OW, Erns RR. 1982. Multiple quantum filters for elucidating NMR coupling networks. *J Am Chem Soc* 104:6800–6801.
- Pope B, Way M, Weeds AG. 1991. Two of the three actin-binding domains of gelsolin bind to the same subdomain of actin: Implications for capping and severing mechanisms. *FEBS Lett* 280:70–74.
- Pope B, Maciver S, Weeds AG. 1995. Localization of the calcium-sensitive actin monomer-binding site in gelsolin to segment 4 and identification of calcium binding sites. *Biochemistry* 34:1583–1588.
- Powers R, Gronenborn AM, Clore GM, Bax A. 1991. Three-dimensional triple-resonance NMR of $^{13}\text{C}/^{15}\text{N}$ -enriched proteins using constant-time evolution. *J Magn Reson* 94:209–213.
- Richardson JS, Richardson DC. 1988. Amino acid preferences for specific locations at the ends of α helices. *Science* 240:1648–1652.
- Schnuchel A, Wiltscheck R, Eichinger L, Schleicher M, Holak TA. 1995. Structure of severin domain 2 in solution. *J Mol Biol* 247:21–27.
- Senn H, Werner B, Messerly BA, Weber C, Traber R, Wüthrich K. 1989. Stereospecific assignment of the methyl ^1H NMR lines of valine and leucine in polypeptides by nonrandom ^{13}C labelling. *FEBS Lett* 249:113–118.
- Szyperski T, Neri D, Leiting B, Otting G, Wüthrich K. 1992. Support of ^1H NMR assignments in proteins by biosynthetically directed fractional ^{13}C labeling. *J Biomol NMR* 2:323–334.
- Vuister GW, Bax A. 1993. Quantitative J correlation: A new approach for measuring homonuclear three-bond J(H^1H^2) coupling constants in ^{15}N -enriched proteins. *J Am Chem Soc* 115:7772–7777.
- Way M, Matsudaira P. 1993. The secrets of severing? *Curr Biol* 3:887–890.
- Way M, Pope B, Weeds AG. 1992. Evidence for functional homology in the F-actin binding domains of gelsolin and α -actinin: Implications for the requirements of severing and capping. *J Cell Biol* 119:835–842.
- Way M, Weeds AG. 1988. Nucleotide sequence of pig plasma gelsolin: Comparison of protein sequence with human gelsolin and other actin-severing proteins shows strong homologies and evidence for large internal repeats. *J Mol Biol* 203:1127–1133.
- Yin HL, Tida K, Janmey PA. 1988. Identification of a polyphosphoinositide-modulated domain in gelsolin which binds to the sides of actin filaments. *J Cell Biol* 106:805–812.